MASTER MASTER

METAL VAPOR EXCIMER LASER

Quarterly Progress Report
for period February 1, 1978 — April 30, 1978

M.A. Kovacs and J.H. Jacobs

AVCO EVERETT RESEARCH LABORATORY, INC.
a Subsidiary of Avco Corporation
Everett, Massachusetts 02149

June 1978

DISCLAIMER

DISCLAIMER

Portions of this document may be illegible in electronic image products. Images are produced from the best available original document.

METAL VAPOR EXCIMER LASER

Quarterly Progress Report
for Period February 1, 1978 - April 30, 1978

M. A. Kovacs and J. H. Jacob

AVCO EVERETT RESEARCH LABORATORY, INC.
a Subsidiary of Avco Corporation
Everett, Massachusetts 02149

Contract No. ES-77-C-02-4275

June 1978

prepared for

THE U. S. DEPARTMENT OF ENERGY
9800 South Cass Avenue
Argonne, Illinois 60439

THIS PAGE
WAS INTENTIONALLY
LEFT BLANK

TABLE OF CONTENTS

THIS PAGE
WAS INTENTIONALLY
LEFT BLANK

LIST OF ILLUSTRATIONS

I. INTRODUCTION AND SUMMARY

Major effort was expended in the final assembly of the gain experiment apparatus; this phase had been delayed by some magnet and discharge tube problems which have now been solved. The addition of the discharge circuitry, now underway, is the last step before gain and discharge tests. The metal testing oven is complete and preliminary tests are underway which show encouraging results concerning the compatibility of mercury vapor and Inconel and 316 SS. Some initial modeling was done with the Boltzmann/kinetics code which demonstrates $CdHg^*$ production efficiency as a function of E/N.

THIS PAGE
WAS INTENTIONALLY
LEFT BLANK

II. EXPERIMENTS

A. E-BEAM DEPOSITION VS DISTANCE

As a continuation of the energy deposition measurements reported in the last quarterly, we determined that energy loss as a function of distance is reduced for a larger diameter confining tube. With the same configuration as in the earlier tests, except the quartz tube was 5 instead of 3 cm in diameter (see Figure 1), we determined the energy remaining in e-beam as a function of distance along the tube axis. Figure 2 shows data for the 3 and 5 cm diameter tubes, both with and without a guide magnetic field, as measured with a central calorimeter, a disk 3 mm in diameter, which measures the axial energy density. Since this calorimeter primarily reflects the behavior of electrons near the axis which would not be seriously affected by the walls, the rate of energy loss with distance does not change much with increasing diameter. (Note: the central calorimeter actually responds to those electrons off the axis which have a large enough Larmor radius to pass through the central region of the tube.) Figure 3 shows data for the large diameter calorimeter (2.5 cm) in 3 and 5 cm tubes, respectively. In the 5 cm case, the energy loss at large distance is less rapid since fewer electrons have a combination of a guiding center far from the axis and a Larmor radius such that the sum of these two distances is greater than the tube radius. These data demonstrate that for a longer discharge length or more uniform energy deposition, one should increase the tube diameter, if one is constrained by magnetic field limitations.

FEBETRON

BRASS TUBE CARRYING
THERMOCOUPLE LEADS

5 cm 2.5 cm PLASTIC PISTON

7.5 cm

TO μ VOLTMETER

3 cm

E-BEAM FOIL

ALUMINUM CALORIMETERS

MAGNET (typ)

H4216

-4-
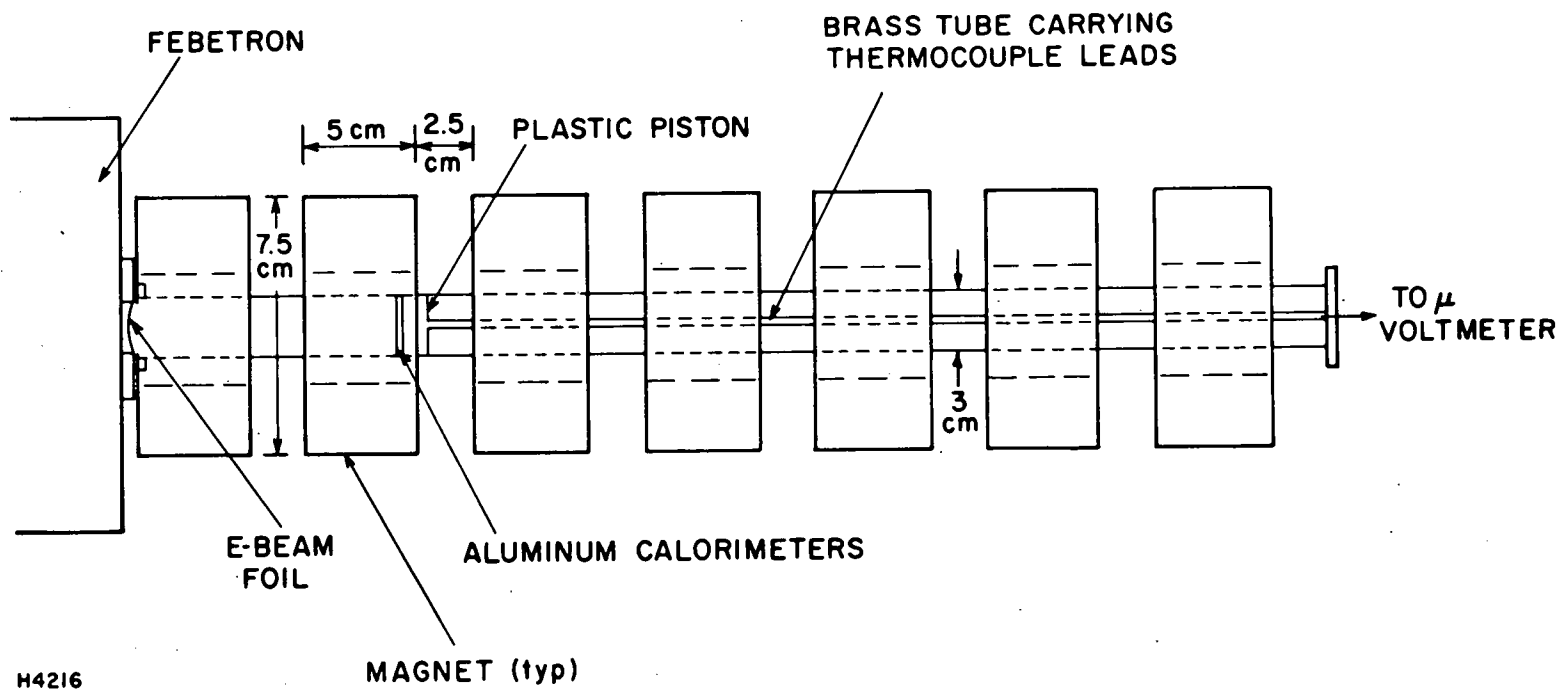
Figure 1   Schematic for Energy Deposition Experiments with Febetron 736
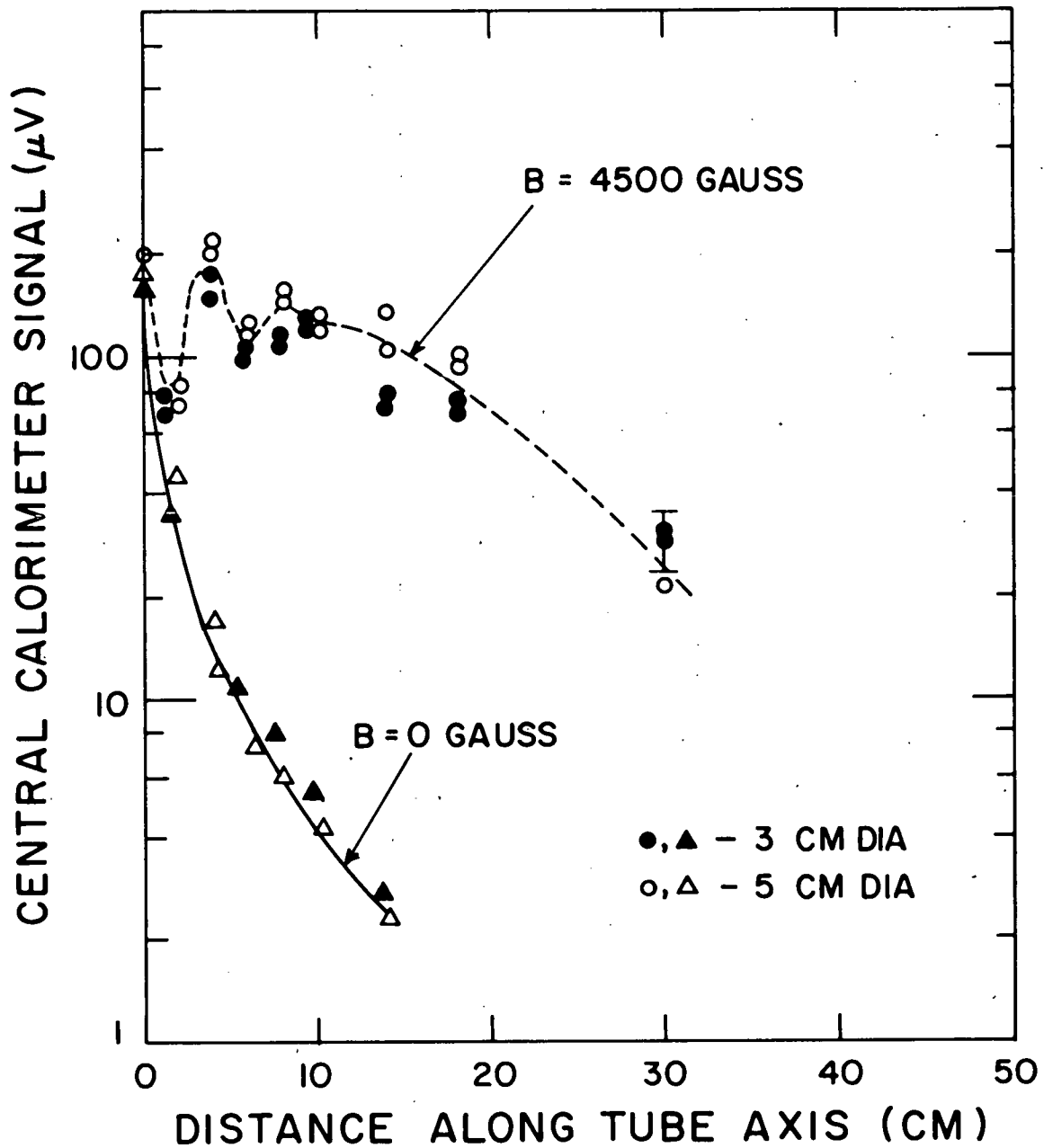
Figure 2   Central Calorimeter Signal vs Distance Along Tube Axis for
3 and 5 cm Guide Tubes

H 5342
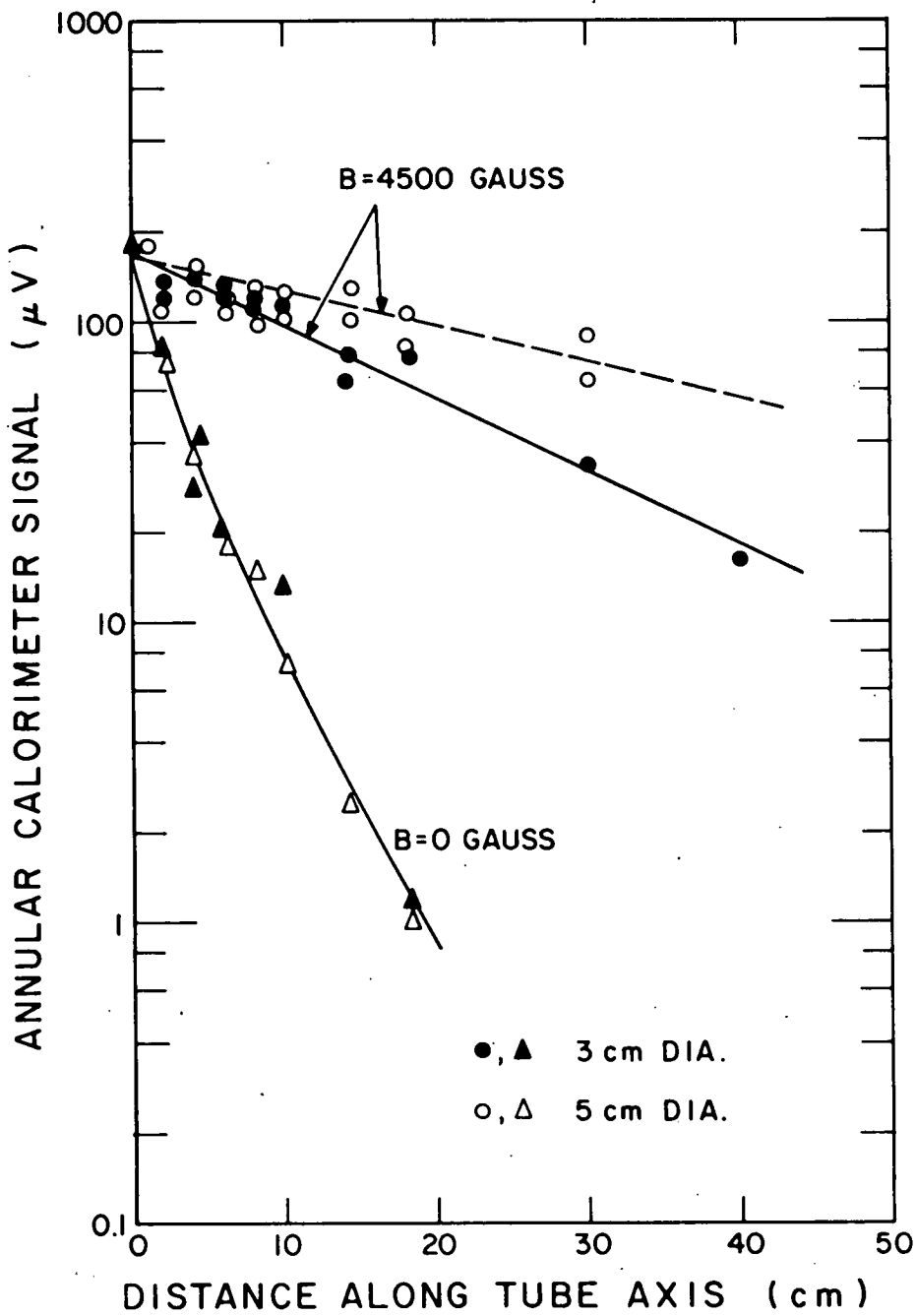
Figure 3   Annular Calorimeter Signal vs Distance Along Tube Axis for 3 and 5 cm Guide Tubes

B. HIGH TEMPERATURE MAGNET TESTS

In the initial high temperature tests of the full magnet assembly (Figure 4), we experienced some problems at the interconnection points between individual magnet coils which eventually led to arc formation which, in turn, destroyed a portion of one magnet coil. This problem was traced to two sources: excessive motion of magnet coils relative to one another and high resistance of the interconnecting tabs. When a large current was turned on, the large magnetic forces stressed the copper interconnecting tabs excessively; this problem was accentuated by the reduced strength of copper at elevated temperatures. Since these tabs had a small cross sectional area, the resistive heating became significant and increased the copper's temperature above the ambient $550^{\circ}C$ test conditions. At 1500 amp the temperature rise per sec was $67^{\circ}C$.

The damaged coil was replaced and all the magnet coils were modified with the addition of a 0.125" thick by 1" wide interconnecting tab (previous dimensions were 0.060" x 0.5"). Furthermore stainless steel straps were used to reduce magnet motion when the current was applied. Figure 5 shows the completed magnet assembly fitted on the quartz discharge tube.

C. E-BEAM GUIDING

In this quarter, we have demonstrated guiding of the e-beam through a 45° angle into the longitudinally excited discharge volume. Figure 6 demonstrates the results of field calculation (reported last quarter) for our particular magnet configuration. The initial magnet alignment was refined using a low pressure dc helium discharge operating in the negative glow

PLAN VIEW
OPTICAL CAVITY OVEN
(LID REMOVED)

Figure 4   Schematic for Full Magnet Assembly Used on Longitudinal
              Discharge Tube

Figure 5   Photograph of Assembled Magnet Assembly and Quartz
Discharge Tube

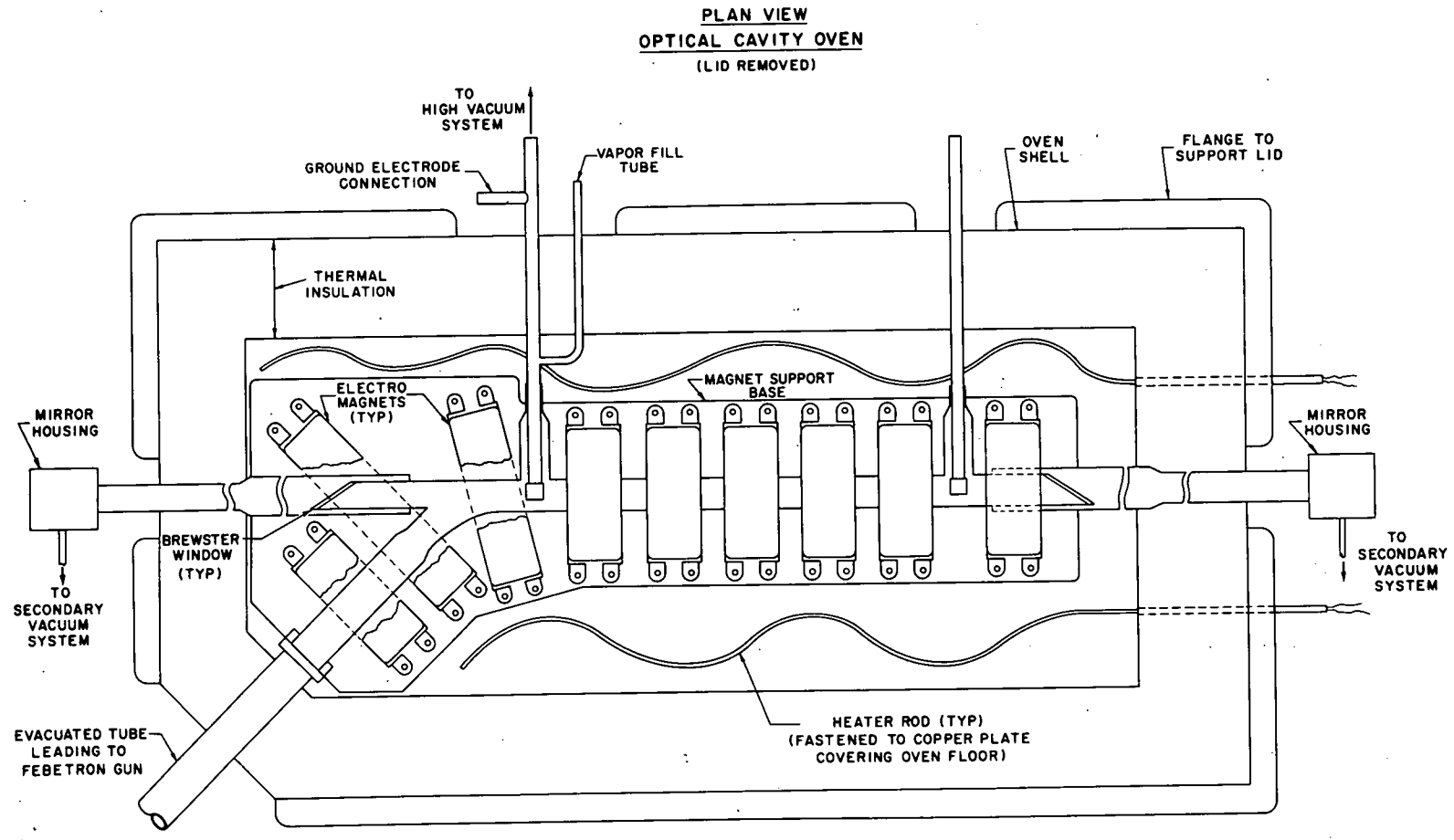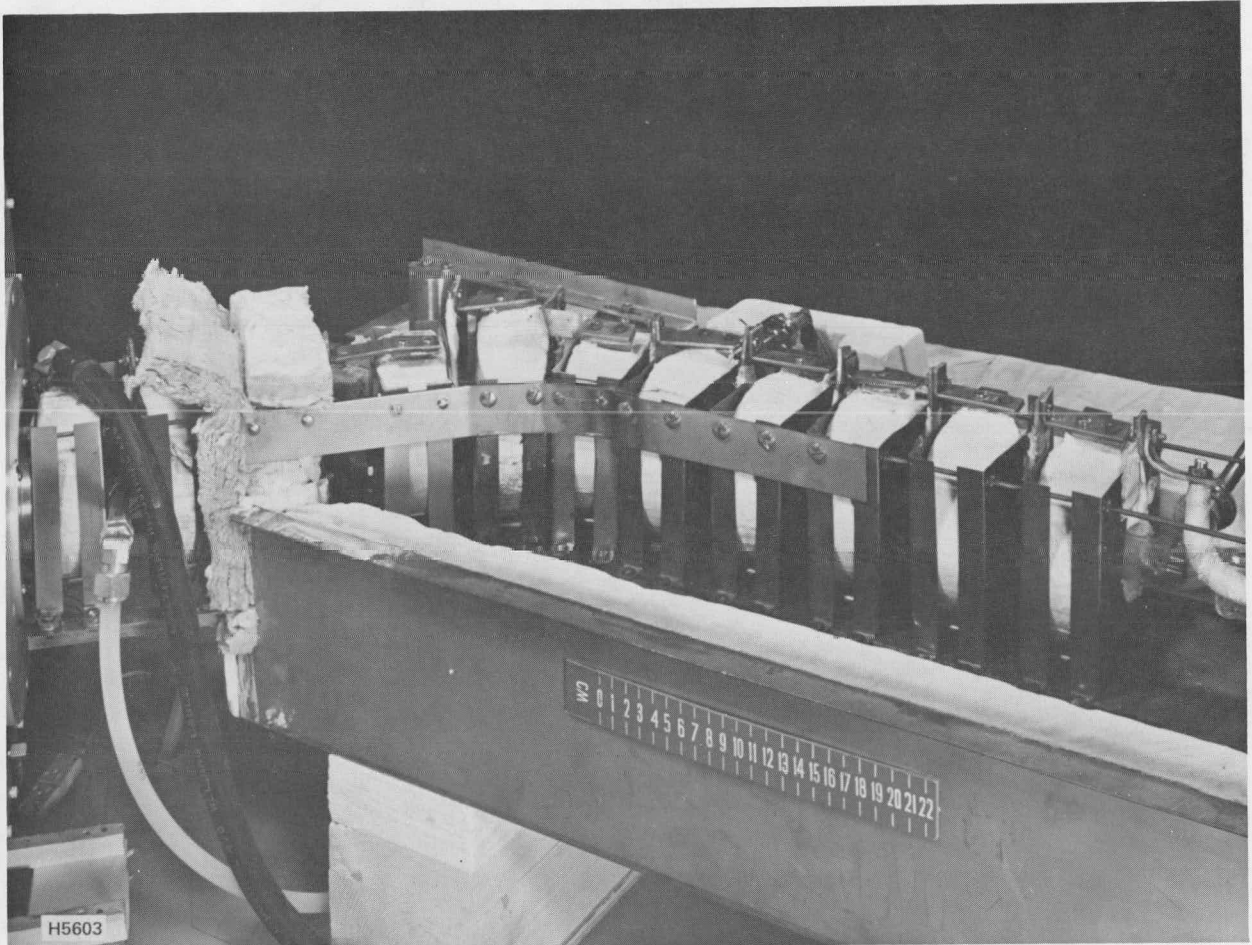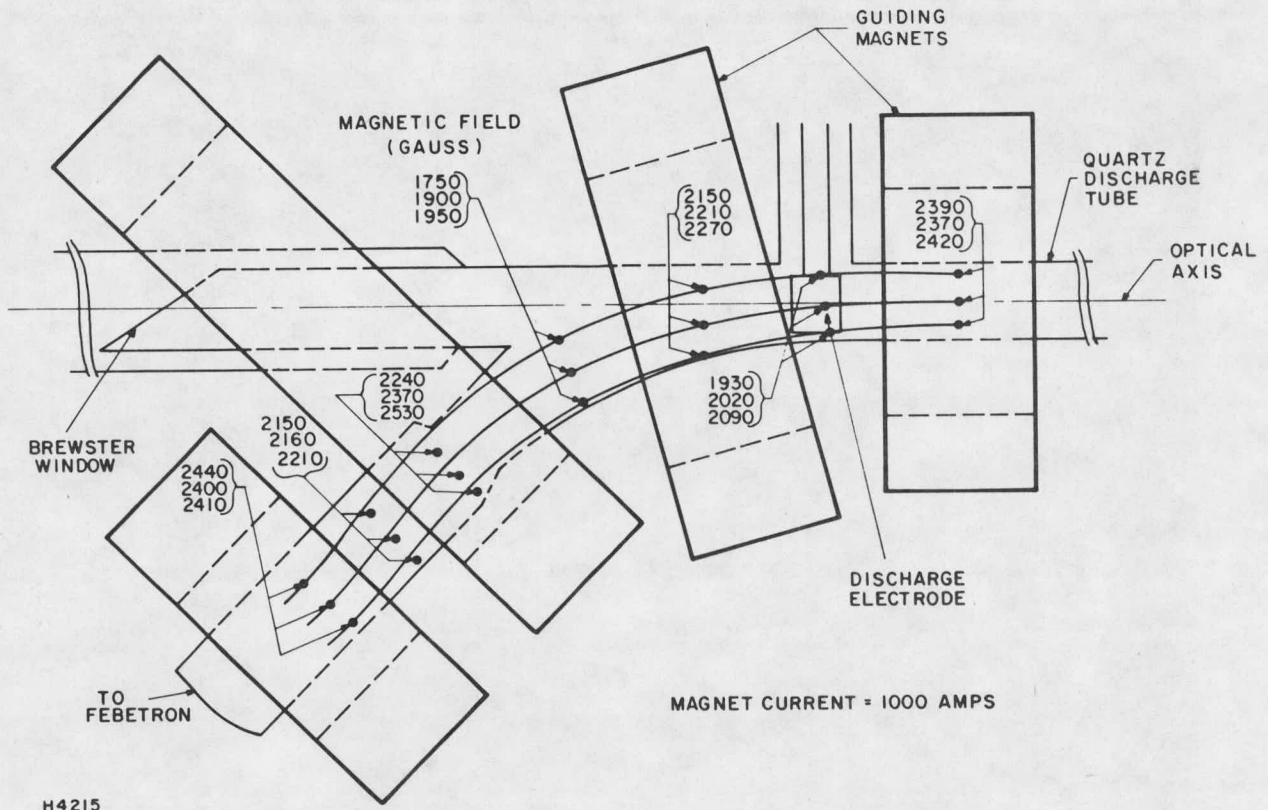Figure 6   Calculated Magnetic Field Distribution in Bending Section; All
Fields Measured in Gauss

region where the electrons can have a very long range (20-30 cm) at pressures below 1 torr. In this low collision region, the electrons are guided along the magnetic field lines and the resulting discharge responds to small perturbations in the magnetic field direction. Figure 7 shows the bending of the low pressure dc discharge with a magnetic field of 750 G (I_{magnet} = 250 amp).

Figures 8a and b exhibit the bending of the Febetron 736 e-beam (electron energy = 500 keV) by the same magnet configuration; there is a 250 torr background pressure of argon in the tube, typical of the density ($\sim 1 \times 10^{19}/cm^3$) which will be used in the gain experiments. In Figure 8a, the magnetic field is zero and the beam strikes the tube in the bend section. At 4500 G, the electrons make the bend and proceed through at least 3 magnet sections (25 cm min).

D. BERYLLIUM FOIL TESTS

The metal vapor gain experiment requires the use of beryllium foil as an e-beam window under operating conditions at $550^{o}C$ and a pressure differential of 2 atm. Lifetime of the foil in these circumstances depends on long-term creep effects for which no data exists. Short-term ($\approx$ 15 min) creep data is published by Kawecki Berylco for cross-rolled sheet under constant stress but this is not directly applicable to foil according to the manufacturer. In the gain experiment apparatus the foil is supported by a series of bars and stress is therefore not constant since plastic deformation allows increasing sag between the bars, leading to a considerable reduction in stress in the unsupported span.

The subject test was devised to explore the creep phenomenon and possible lifetime of the foil. The foil used for the test was Kawecki-Berylco

-11-

MAGNETIC FIELD GUIDING OF LOW PRESSURE He DISCHARGE

I = 250 A   B ~ 750 GAUSS

H 4369

Figure 7   Bending of Low Pressure Helium Discharge.   Magnetic Field
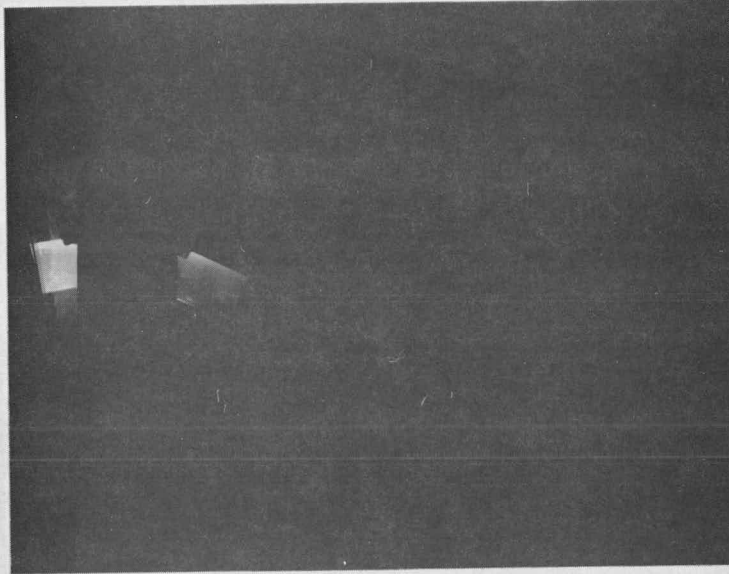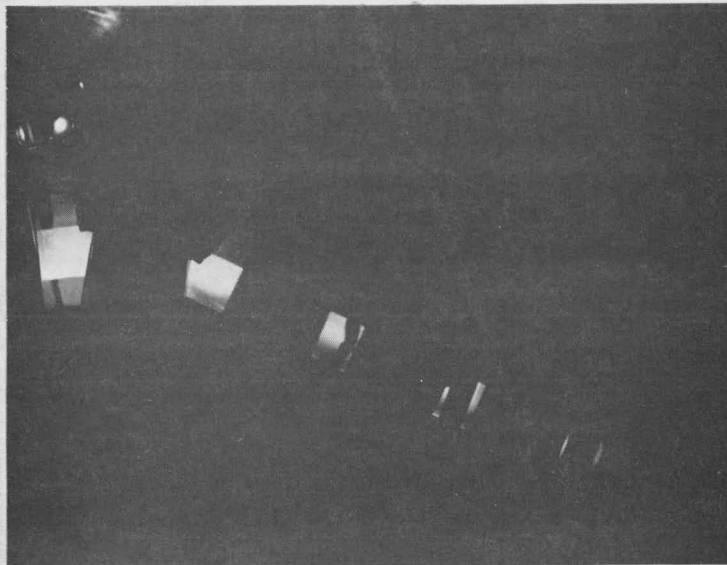is 750 G at 250 amps.

MAGNETIC FIELD GUIDING OF FEBETRON E—BEAM
(250 TORR ARGON — 500 keV ELECTRONS)

B = 0

B = 4500 GAUSS

H4370

Figure 8   Bending of 500 keV E-Beam Passing Through Argon Buffer
Gas. (a) No Magnetic Field, (b) Magnetic Field = 4500 G.

high purity grade 1F-1, 0.002" thick, supported by bars 0.034" wide at 0.084" spacing. Creep was estimated by measuring the amount of sag in the foil (by the method described later) and comparing this with the curves in Figure 9 which are plotted from catenary formulae given in Marks Handbook.[1]

Two curves are shown, one assumes that creep is uniform over the entire surface, the other that it is confined to the unsupported span. It is considered that the former condition may be true for initial deformation but that the latter is more accurate for subsequent observations.

The schematic for the test assembly and foil support is shown in Figure 10. Difficulty was experienced in making the foil vacuum tight with the C-rings called out on the assembly drawing. The rings apparently collapsed into the grooves without exerting sufficient pressure to produce a satisfactory seal. After several unsuccessful attempts these were replaced with annealed copper rings, of square cross section, having a raised ridge ($\approx$ 0.010 x 0.010) on the sealing faces and these enabled a pressure of 25-30 μm to be maintained.

The larger C-rings, at the junction of foil holder and test housing, did perform satisfactorily but did not appear reusable. The silver plating showed a tendency to blister from the heat and, in some cases, to flake off. It is suggested that similar copper crush rings be used here when the present stock is exhausted.

Both sides of the foil were opened to the vacuum pump and the heating units turned on. When operating temperature was reached (typically 1-1/2 to 2 hours) the test housing valve was closed and a differential pressure of 30 psi applied to the foil. As the helium temperature increased it
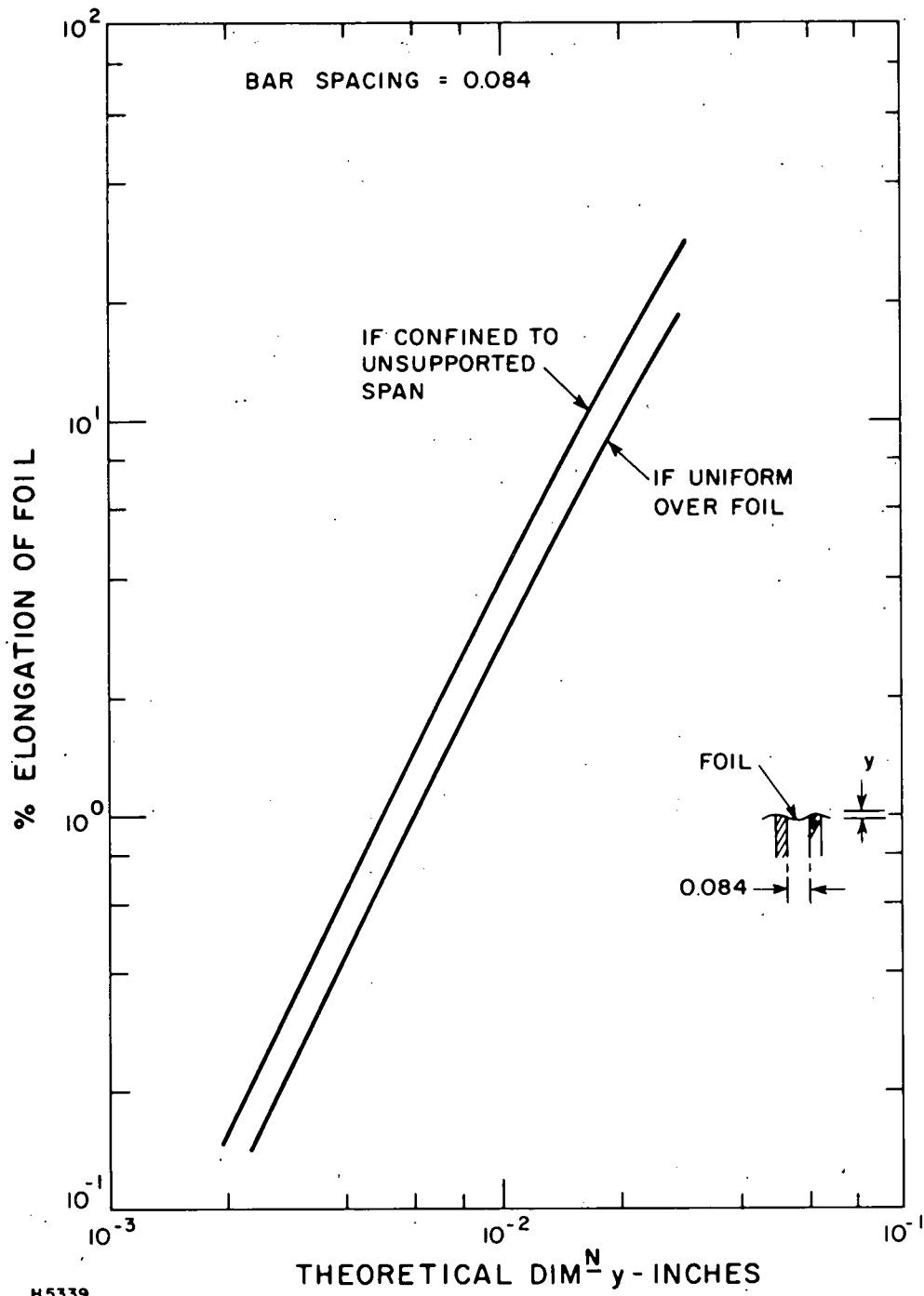
Figure 9   Calculated Percentage Elongation of Beryllium Foil as a
            Function of Sag

CLAMPING PIECES

FOIL HOLDER ASS'Y

TEST HOUSING ASS'Y

COPPER SEAL (TYP)

RETAINING NUT

C-RING SEAL

FOIL SUPPORT

KEYED WASHER

FOIL

SEAL GROOVES

0.034 (TYP)

0.042

0.90 DIA

0.084 (TYP)
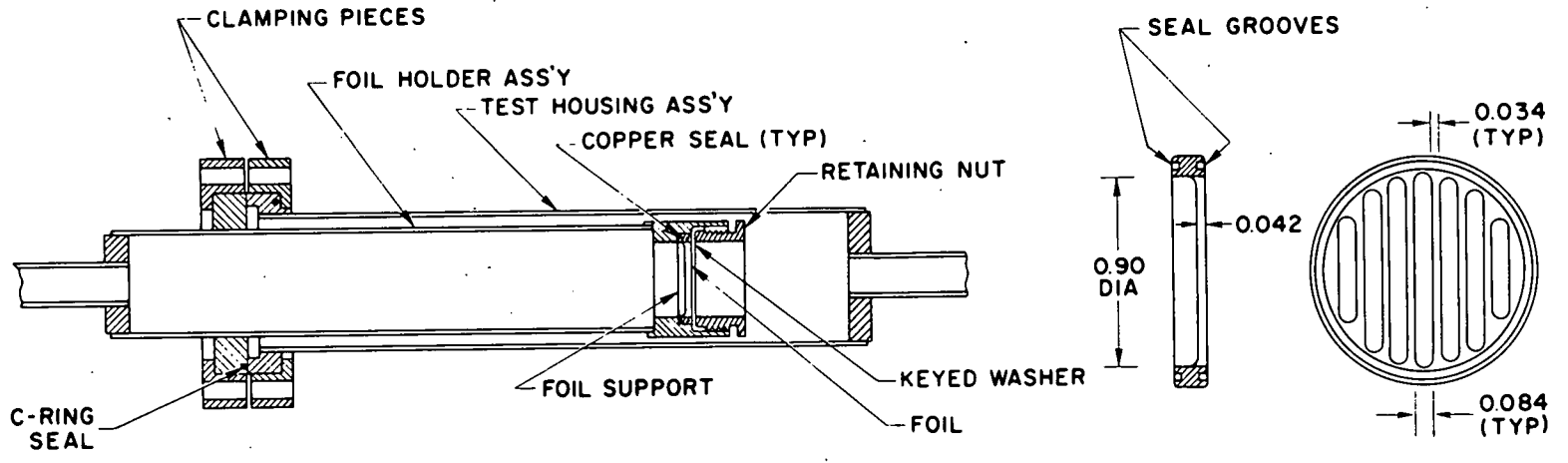
H5575

Figure 10   Schematic for Foil Test Assembly

-16-

was necessary to use the bleed valve to keep the pressure constant until a stabilized condition was reached. At the end of each test period, the assembly was allowed to cool, the foil holder removed, and the depression of the foil measured. This measurement was made on a lathe bed on which a fine probe (actually one lead of an ohmmeter) was attached to the tool post while the foil holder was mounted on the chuck. When contact was made (open to finite resistance circuit) the position was read from the tool slide. With this method we could make precise measurements without disturbing the foil.

A series of five measurements were taken with the results shown in Figure 11. Testing was halted after 32 hours as scheduling did not permit further experimentation.

The stress vs elongation curve in Figure 11, also calculated from catenary formulae, shows the marked reduction in stress occuring in the early stages of deformation. This accounts for the changes in slope of the time vs elongation curve and it is unfortunate that time did not permit more, shorter test periods to define this more closely.

At the conclusion of the tests the foil was still in good condition and, visually, appeared unchanged from the first inspection at 1-1/4 hours, neither had it become very brittle, as had been expected. Some discoloration from the heating was noted but the foil is considered to be still usable.

E. MATERIALS TEST OVEN

The materials testing oven, which is required under Task VI, has been assembled and is operating. This small oven (see Figure 12 for a schematic) provides apparatus for testing materials and components exposed to mercury or cadmium metal vapors. The two compartments give one the flexibility to set the vapor pressure and temperature independently.
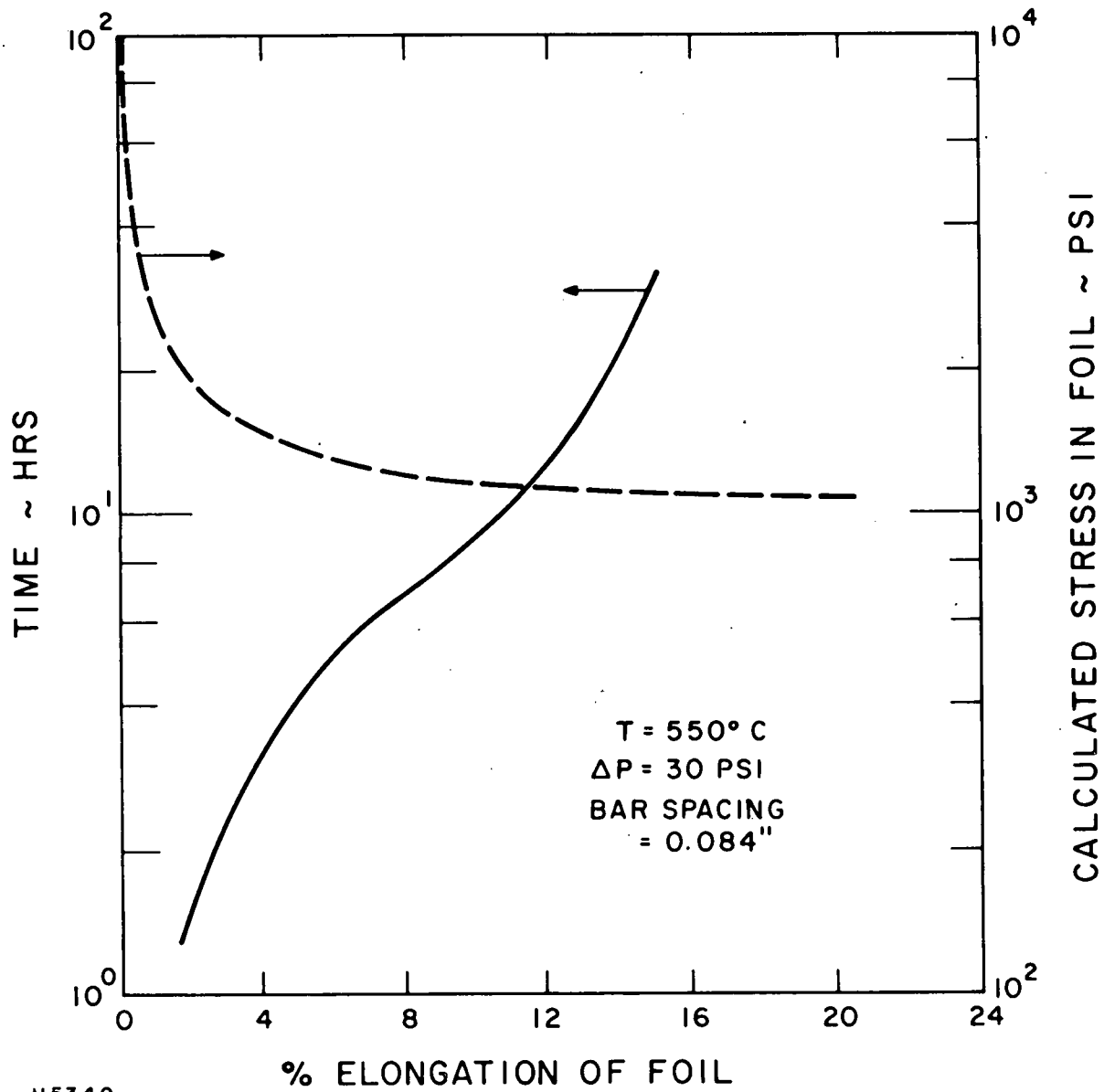
Figure 11   Results of Creep Test on 2 mil Heated Beryllium Foil

H5340
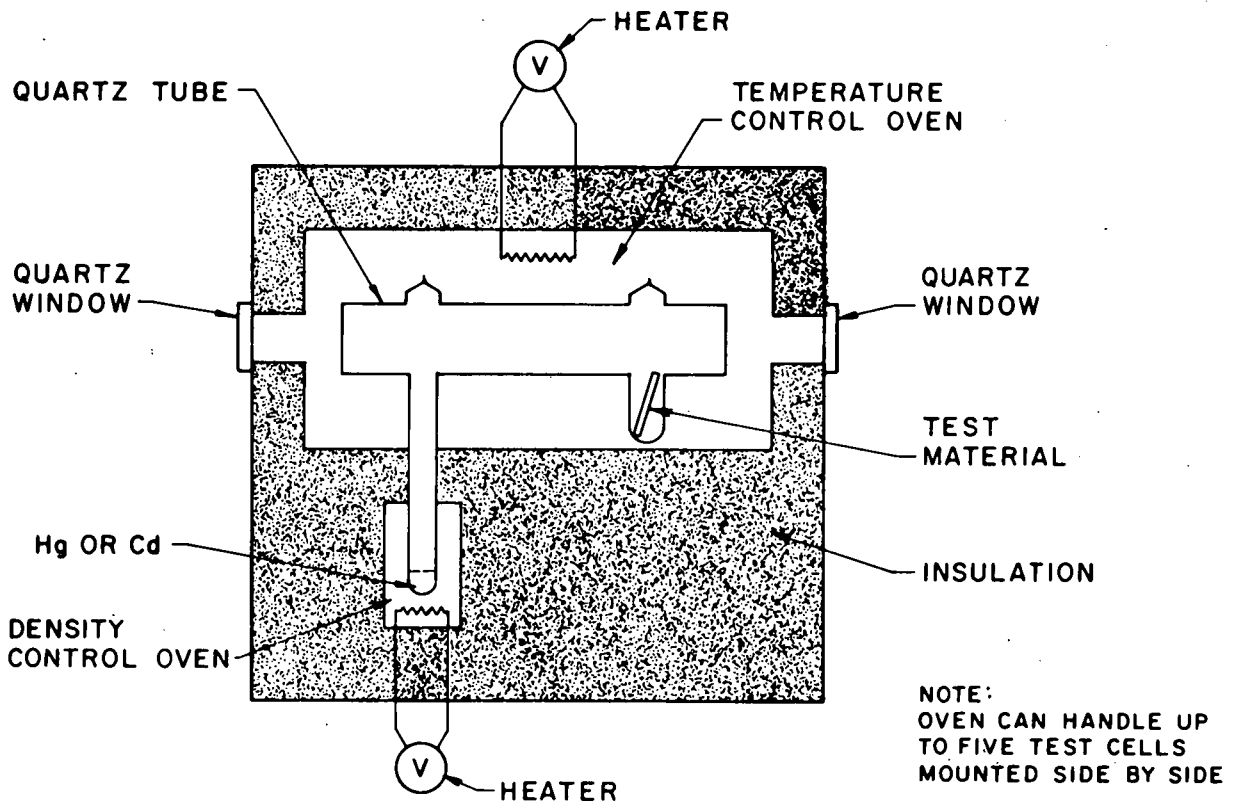
Figure 12   Schematic of Materials Test Oven Set Up for Corrosion Testing

Tests are presently planned using two configurations. In the materials testing phase -- identifying which materials can resist mercury and cadmium corrosion at temperatures above 500°C -- we will place small, clean samples of various metals, e.g., stainless steel, Inconel, Monel, etc. each in a quartz test ampule (Figure 12) which contains either Hg, Cd or an amalgam of both. The long "finger" will sit in the lower oven compartment which will control the vapor pressure while the remainder of the ampule will be in the upper compartment where the higher temperatures will determine the test conditions. Each ampule will be filled, evacuated, sealed, heated, and finally opened for inspection of the sample materials. By observing surface degradation and weight loss we should be able to determine how well the test material would endure in a high temperature metal vapor environment.

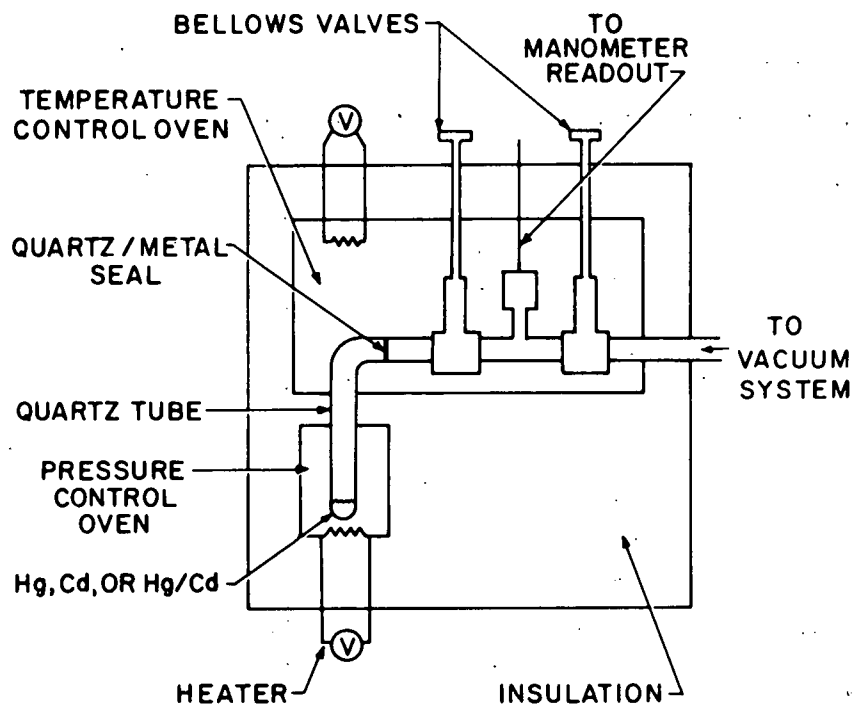The second test configuration (see Figure 13) is aimed at testing individual vacuum system components. Presently a high temperature manometer (Kaman Sciences Model KP 1910 rated for operation at 540°C) is located in the upper oven and is being checked for its ability to withstand Hg and Cd. We are concerned that amalgams may form with component materials, thereby consuming the mercury or cadmium. The high temperature manometer would make an excellent tool for recording pressure as a function of time in subsequent materials tests -- provided that the manometer materials themselves do not react with Hg or Cd. Thus far tests with Hg vapor show little pressure loss with time. Hg vapor was allowed into the manometer volume ($\sim 3 \ cm^3$) and sealed off with a stainless steel bellows valve both of which were at 475°C. The pressure was then recorded as a function of time over a 4 minute interval (see Figure 14). In the same figure

BELLOWS VALVES

TO MANOMETER READOUT

TEMPERATURE CONTROL OVEN

QUARTZ / METAL SEAL

TO VACUUM SYSTEM

QUARTZ TUBE

PRESSURE CONTROL OVEN

Hg, Cd, OR Hg/Cd

HEATER

INSULATION

H 5337

Figure 13   Schematic of Materials Test Oven Set Up for Testing the High Temperature Manometer
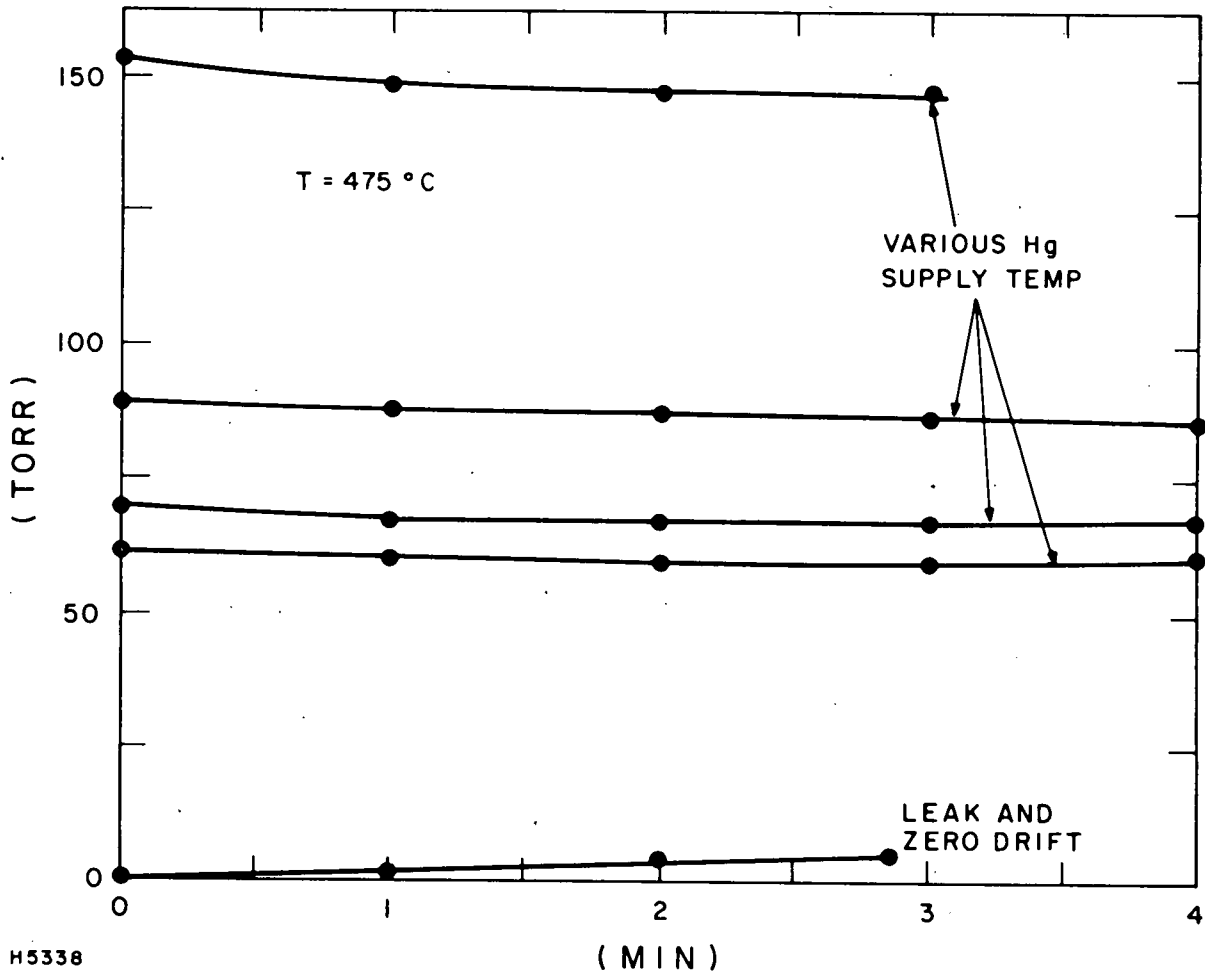
Figure 14   Measured Hg Pressure in Sealed Off Manometer Volume as a
Function of Time for Several Initial Mercury Pressures

is the combined leak and zero drift data for an initially evacuated manometer volume. Although these measurements represent a composite of losses occurring in the manometer volume (Inconel) and bellows valve (316 SS), they show a very small total effect over periods typical of any present experiment. There was initial concern that mercury vapor placed in the gain experiment apparatus would rapidly disappear before adequate mixing occurred and a gain measurement could be made. This very preliminary data suggests that this may not be a problem for Hg vapor, at least. These tests are continuing with Cd; in addition the data will be analyzed in terms of diffusion and wall loss in order to make more quantitative statements about metal vapor losses with various structural materials.

F. FINAL ASSEMBLY

During this quarter we completed final assembly of the discharge tube, magnet assembly and heated fill lines (see Figure 15). This task was delayed in part due to quartz tube fracture during insertion of the Be foil vapor barrier assembly. The final step before experiments can begin is addition of the discharge circuitry -- a step now underway.

The entire assembly can be maintained at 575°C through a series of heaters and temperature controllers. The fill line section is encased in a copper jacket covered by ceramic insulation to insure a uniform temperature distribution over the length between the discharge tube and vapor supply oven. The discharge tube oven is fitted with an insulated lid (not shown) having an air spaced quartz window to monitor sidelight emission.
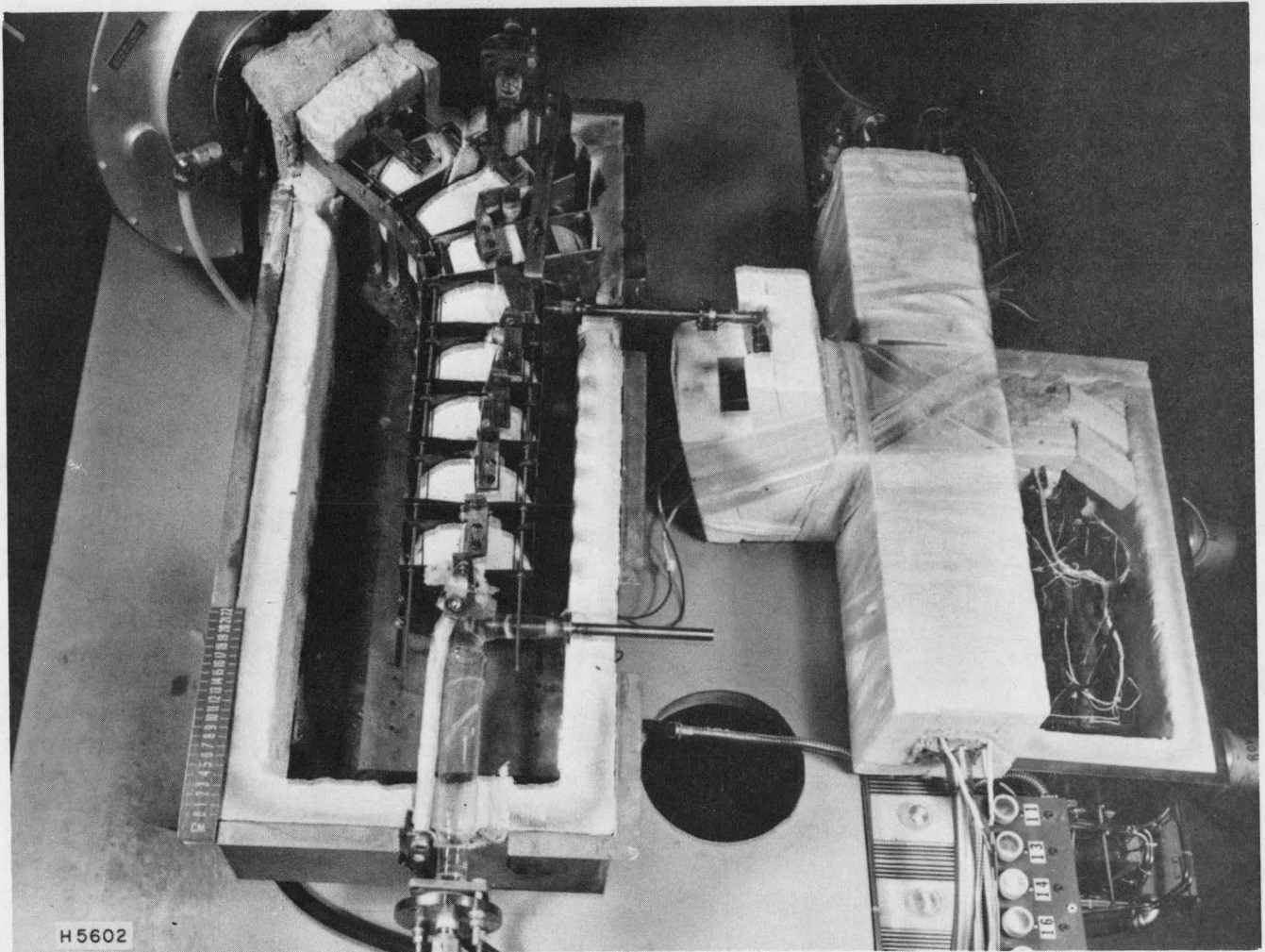
-23-

Figure 15   Completed Assembly of Discharge Pumped Gain Experiment.
The discharge circuitry fits in the hole at the lower right of
the photo.

III. KINETICS MODELING

We have begun some calculations using the full Boltzmann/kinetics code[2] in which we have calculated the $CdHg^*$ density and $CdHg^*$ production efficiency for several E/N values. These calculations included the kinetic processes listed in Table 1 with the known and estimated rates specified. Excluded from these calculations were electron and three body quenching rates for $CdHg^*$. Although these data are unknown, we are beginning a series of calculations checking the overall sensitivity of the $CdHg^*$ production to these rates.

Figures 16 and 17 show the $CdHg^*$ density and production efficiency at a total density of 1.2 and 4.8×10^{19} atoms/cm^3 respectively for a mixture 1:0.2:0.02 Ne:Hg:Cd. The production efficiency rises sharply at higher density since the increased three body production rate for $CdHg^*$ leads to a more favorable branching ratio for transfer of Cd^* atoms to $CdHg^*$ molecules. This same effect is also responsible for the discharge remaining stable in the 2000 V/cm case compared to the similar lower pressure example; energy is directed from the ionization pathway into excimer formation thereby lowering the possibility of an avalanche. This benefit clearly has a limit which is determined by the as yet unknown quenching rates such as

$$CdHg^* + Hg + M \rightarrow CdHg_2^* + M$$

If this rate is as rapid as that thus far determined for mercury trimer formation,[3]

TABLE 1

KINETIC RATES USED IN INITIAL CALCULATIONS

Electron Kinetics	Rate Constant[*]
$Cd + e \rightarrow Cd^* + e$	Boltzmann code
$Cd^* + e \rightarrow Cd^{**} + e$	Boltzmann code
$Cd^{**} + e \rightarrow Cd^* + e$	1.2×10^{-7} (Boltzmann code)
$Cd^* + e \rightarrow Cd + e$	8.4×10^{-8} (Boltzmann code)
$Cd_2^* + e \rightarrow 2\,Cd$	1×10^{-7} cm^3/sec
$Hg + e \rightarrow Hg^* + e$	Boltzmann code
$Hg^* + e \rightarrow Hg^{**} + e$	0
$Hg^* + e \rightarrow Hg + e$	0
$Hg^{**} + e \rightarrow Hg^* + e$	0
$Hg_2^+ + e \rightarrow 2\,Hg$	1×10^{-7} cm^3/sec

Heavy Particle Kinetics	
$Cd^* + Hg + M \rightarrow CdHg^* + M$	6×10^{-31} cm^6/sec (Fournier & McGeoch)
$Cd^+ + Cd + M \rightarrow Cd_2^+ + M$	2.5×10^{-31} cm^6/sec
$Cd_2^* + Cd + M \rightarrow Cd_2^* + M$	2.5×10^{-31} cm^6/sec
$CdHg^* + Cd + M \rightarrow Cd_2^* + Hg$	0
$Cd^{**} + Hg + M \rightarrow CdHg^* + M$	0
$CdHg^* + Cd + M \rightarrow Cd_2Hg^* + M$	0
$CdHg^* + Hg + M \rightarrow CdHg_2^* + M$	0
$CdHg^* \rightarrow Cd + Hg + h\nu$	$\tau = 4$ μsec (Fournier & McGeoch)

TABLE 1

KINETIC RATES USED IN INITIAL CALCULATIONS (Continued)

Heavy Particle Kinetics	Rate Constant[*]
$Hg^* + Hg + M \rightarrow Hg_2^* + M$	$2.5 \times 10^{-31} \ cm^6/sec$
$Hg^{**} + Hg + M \rightarrow Hg_2^* + M$	0
$Hg^+ + Hg + M \rightarrow Hg_2^+ + M$	$2.5 \times 10^{-31} \ cm^6/sec$
$Hg_2^* + Hg + M \rightarrow Hg_3^* + M$	0
$Hg_2^* + Cd + M \rightarrow CdHg^* + M$	0
$Hg_2^* \rightarrow 2\,Hg + h\nu$	$\tau = 10\ \mu sec$

[*]The constants labeled Boltzmann code are derived from energy dependent cross section data for cadmium and mercury and appear in the kinetics code as a two dimensional array dependent on the Cd^*/Cd and Cd^{**}/Cd^* ratios. The other rates are generally estimates unless otherwise stated. It is recognized that recently a fairly complete set of mercury data from NBS has become available; this will be included in subsequent calculations.
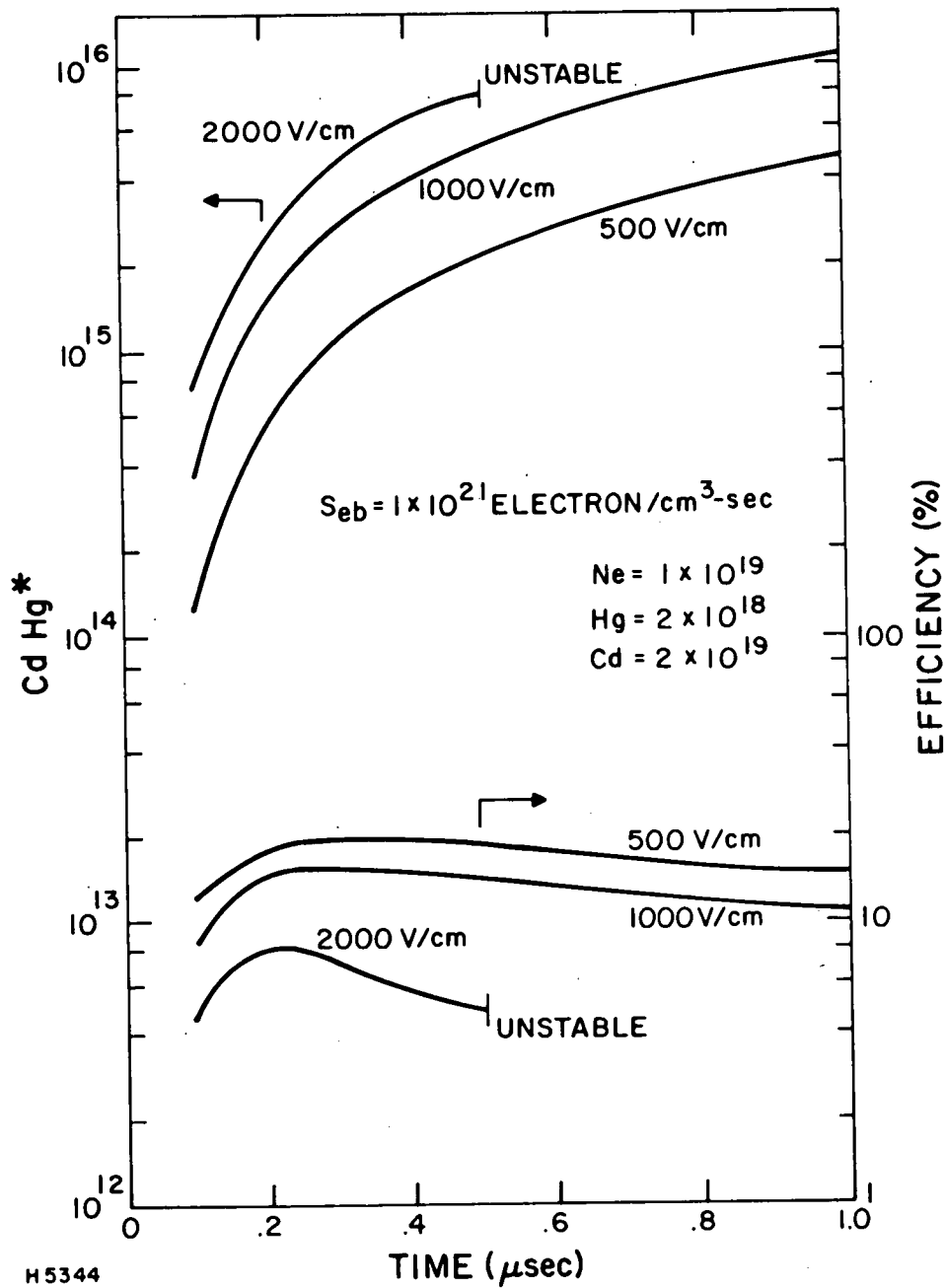
Figure 16   Calculated CdHg* Density and Production Efficiency vs Time for a Rectangular Discharge Pulse (E/N variable) Augmented with an Ionization Source of 1×10^{21} electron/cm^3-sec. Total particle density is 1.2×10^{19}/cm^3.
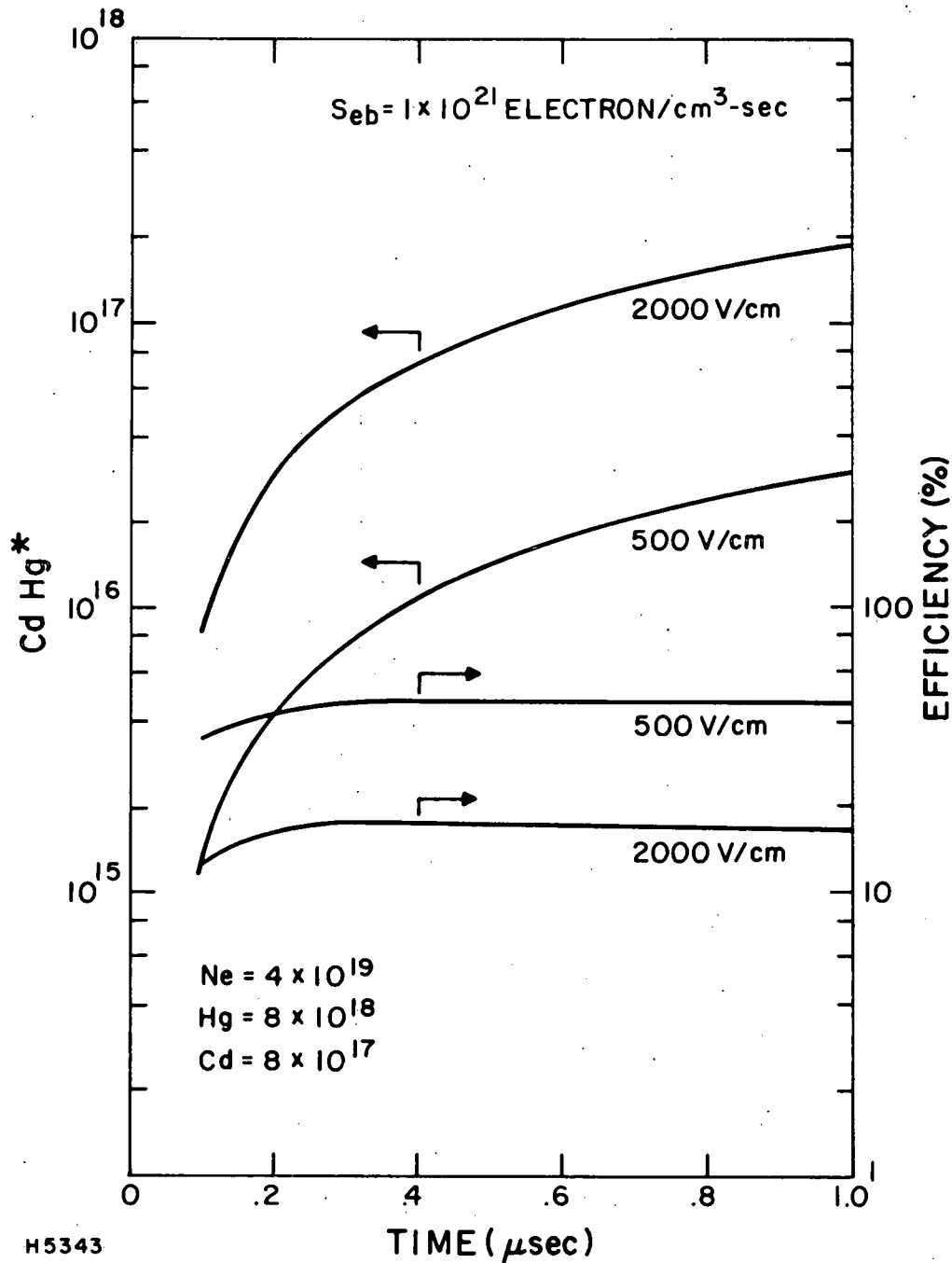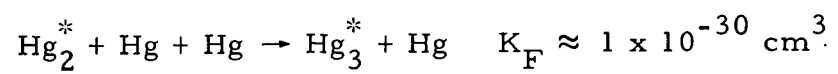
Figure 17   Calculated CdHg* Density and Production Efficiency vs Time
             for a Rectangular Discharge Pulse (E/N variable) Augmented
             with an Ionization Source of 1×10^{21} electron/cm^3-sec. Total
             particle density is 4.9×10^{19}/cm^3.

$$Hg_2^* + Hg + Hg \rightarrow Hg_3^* + Hg \quad K_F \approx 1 \times 10^{-30} \text{ cm}^3$$

an upper bound on the pressure will be rapidly reached and the maximum efficiency could lie well below the calculations here. This evaluation is now underway.

REFERENCES

1. Baumeister, T., and Marks, L., <u>Standard Handbook for Mechanical Engineers</u>, McGraw-Hill, 7th edition, 1967.

2. Srivastava, B.N., Jacob, J.H., Mangano, J.A., and Hsia, J.C., <u>Visible Laser Discharge Studies</u>, Final Technical Report, Department of Energy, Contract #EY-76-C-02-2922, 1977.

3. Mosburg, E.R., <u>Destruction of Hg Excimers by Electrons in a High Pressure Discharge</u>, U.S.-Japan Joint Seminar on Glow Discharge, JILA, July 1977.

DISTRIBUTION LIST

Dr. Paul W. Hoff (6 copies)
New Laser Programs Manager
Office of the Assistant Director
     for Laser Fusion
Division of Laser Fusion C-404
U.S. ERDA
Washington, D.C. 20545

Dr. John L. Emmett
Associate Director for Lasers
Lawrence Livermore Laboratory
P.O. Box 808
Livermore, CA 94550

Dr. Roger B. Perkins
L Division Leader
Los Alamos Scientific Laboratory
P.O. Box 1663
Los Alamos, NM 87545

Dr. James B. Gerardo
Sandia Laboratories
P.O. Box 5800
Albuquerque, N.M. 87115

Dr. Donald Setser
Kansas State University
Department of Chemistry
Manhattan, Kansas 66505

Dr. H. Kildal
Massachusetts Institute of Technology
Lincoln Laboratory
Lexington, MA 02173

Dr. Nicholas I. Djeu
Code 5540
Naval Research Laboratory
Washington, D.C. 20375

Dr. Robert Center
Mathematical Sciences Northwest, Inc.
P.O. Box 1887
Bellevue, WA 98009

Dr. Ray Taylor
Physical Sciences, Inc.
30 Commerce Way
Woburn, MA 01801

Dr. William F. Krupke
Lawrence Livermore Laboratory
L-258
P.O. Box 808
Livermore, CA 94550

Dr. Gerald L. Rogoff
Westinghouse Electric Corporation
1310 Beulah Road
Pittsburgh, PA 15235